The QBO–MJO Connection: A Possible Role for the SST and ENSO

DAVID A. RANDALL,[a] ELI TZIPERMAN,[b,c] MARK D. BRANSON,[a] JADWIGA H. RICHTER,[d] AND WANYING KANG[e]

[a] *Department of Atmospheric Science, Colorado State University, Fort Collins, Colorado*
[b] *Department of Earth and Planetary Sciences, Harvard University, Cambridge, Massachusetts*
[c] *School of Engineering and Applied Sciences, Harvard University, Cambridge, Massachusetts*
[d] *National Center for Atmospheric Research, Boulder, Colorado*
[e] *Department of Earth, Atmospheric and Planetary Sciences, Massachusetts Institute of Technology, Cambridge, Massachusetts*

(Manuscript received 17 January 2023, in final form 1 May 2023, accepted 6 June 2023)

ABSTRACT: We examine the hypothesis that the observed connection between the stratospheric quasi-biennial oscillation (QBO) and the strength of the Madden–Julian oscillation (MJO) is modulated by the sea surface temperature (SST)—for example, by El Niño–Southern Oscillation (ENSO). A composite analysis shows that, globally, La Niña SSTs are remarkably similar to those that occur during the easterly phase of the QBO. A maximum covariance analysis suggests that MJO power and SST are strongly linked on both the ENSO time scale and the QBO time scale. We analyze simulations with a modified configuration of version 2 of the Community Earth System Model, with a high top and fine vertical resolution. The model is able to simulate ENSO, the QBO, and the MJO. The ocean-coupled version of the model simulates the QBO, ENSO, and MJO, but does not simulate the observed QBO–MJO connection. When driven with prescribed observed SST anomalies based on composites for QBO east and QBO west (QBOE and QBOW), however, the same atmospheric model produces a modest enhancement of MJO power during QBOE relative to QBOW, as observed. We explore the possibility that the SST anomalies are forced by the QBO itself. Indeed, composite Hovmöller diagrams based on observations show the propagation of QBO zonal wind anomalies all the way from the upper stratosphere to the surface. Also, subsurface ocean temperature composites reveal a similarity between the western Pacific and Indian Ocean subsurface signal between La Niña and QBOE.

KEYWORDS: Madden–Julian oscillation; Quasibiennial oscillation; Southern Oscillation

1. Introduction

The Madden–Julian oscillation (MJO) is the dominant intraseasonal (30–70-day period) variability in the tropical troposphere, characterized by a convective envelope that propagates slowly eastward at about 5 m s^{-1} (Madden and Julian 1971; Zhang 2005). The MJO affects weather globally, is connected with the Pacific–North America pattern and with blocking events in the midlatitudes (Yoo et al. 2012b, 2011; Cassou 2008), impacts Arctic surface temperatures (Yoo et al. 2012a; Goss et al. 2016), and modulates the occurrence of westerly wind bursts that may amplify or terminate El Niño events (Harrison and Schopf 1984; McPhaden 1999; Yu et al. 2003; Seiki and Takayabu 2007; Eisenman et al. 2005; Miyakawa et al. 2017). The MJO is projected to become stronger in a warmer climate (Slingo et al. 1999; Subramanian et al. 2014; Jones and Carvalho 2006; Oliver and Thompson 2012; Liu et al. 2013; Schubert et al. 2013; Arnold et al. 2014, 2015; Rushley et al. 2019; Bui and Maloney 2018), and such a strengthening may lead to more frequent Arctic polar vortex collapses (Kang and Tziperman 2017, 2018). Predicting the interannual variability of the MJO is, therefore, key to improving subseasonal-to-seasonal forecast skill (Meehl et al. 2021).

A relationship between the MJO and the stratospheric quasi-biennial oscillation (QBO) has recently been identified in observations (Yoo and Son 2016; Zhang and Zhang 2018; Nishimoto and Yoden 2017; Marshall et al. 2017; Son et al. 2017; Martin et al. 2021c). The QBO involves alternating zonal easterlies and westerlies (hereinafter QBOE and QBOW) throughout the tropical stratosphere and in particular at 50 hPa. The observed average period of the QBO is approximately 28 months (Baldwin and Dunkerton 2001). When QBOE occurs during boreal winter, the MJO-power calculated as in Wheeler and Kiladis (1999) becomes 40% stronger, MJO events are triggered more often and propagate farther east from the Indian Ocean into the mid-Pacific (Zhang and Zhang 2018; Martin et al. 2021c). Information about the phase of the QBO has been shown to significantly improve forecasts of MJO power (Marshall et al. 2017). For convenience, we refer to these observed relationships as the QBO–MJO connection.

The mechanism of the QBO–MJO connection is not clear (Martin et al. 2021c). Thus far, most proposed mechanisms have focused on the QBO's effects on upper-tropospheric stratification. According to the thermal wind balance, the lowermost equatorial stratosphere should have a cold anomaly during QBOE, leading to weakened stratification near the tropopause, which in turn may enhance the deep convection associated with the MJO. This hypothesis has been examined in a cloud-resolving regional model with a parameterized large-scale circulation (Martin et al. 2019) and in a weather forecasting model (Martin et al. 2020). However, a general circulation model (GCM) did not simulate this mechanism (Martin et al. 2021a). Since the QBO-induced temperature anomalies alone seem insufficient to

Denotes content that is immediately available upon publication as open access.

Corresponding author: David A. Randall, david.randall@colostate.edu

DOI: 10.1175/JCLI-D-23-0031.1

explain the observed modulation of the MJO (Martin et al. 2021b; Huang et al. 2023), it has been proposed that the radiative cooling associated with increased cirrus clouds during QBOE can further destabilize the tropopause and enhance convection and the MJO (Son et al. 2017; Sakaeda et al. 2020; Lin and Emanuel 2023). These hypotheses have yet to be tested due to deficiencies of GCM-simulated clouds and gravity waves, and because none of the currently available GCMs can reproduce the observed link between the QBO and the MJO (Lee and Klingaman 2018; Lim and Son 2020; Kim et al. 2020; Martin et al. 2021c).

El Niño–Southern Oscillation (ENSO) also affects the strength, propagation, and location of the MJO (Tang and Yu 2008; Chen et al. 2015; Pang et al. 2016; Wang et al. 2018; Sun et al. 2019). During La Niña, the western Pacific MJO and the easterly QBO phase are both stronger (Sun et al. 2019). During El Niño years, if the warming signal is concentrated in the central Pacific (CP El Niño), the MJO is strengthened (Pang et al. 2016). If the warming spreads to the east Pacific (EP El Niño), the MJO is weakened instead. This is consistent with observations showing that the MJO weakened during the strong El Niño events of 1982/83 and 1997/98 (Hendon et al. 1999). The QBO wind anomalies are weaker and propagate downward more rapidly during El Niño (Taguchi 2010). In addition, the phase of the QBO winds does respond to strong El Niño forcing in a numerical simulation (Christiansen et al. 2016). Analysis of observations for 1957–2007 shows that the response of the QBO to strong El Niño forcing emerges after 1979 when the relevant satellite measurements became available (Garfinkel and Hartmann 2007). These suggested connections between ENSO, the MJO, and the QBO lead us to hypothesize that the observed QBO–MJO correlation may stem from their individual connections with ENSO or, more generally, with the SST.

In this work, we utilize both observations and simulations to investigate mechanisms by which the SST might play a role in the observed QBO–MJO connection (Yoo and Son 2016; Zhang and Zhang 2018; Nishimoto and Yoden 2017; Marshall et al. 2017; Son et al. 2017; Martin et al. 2021c). Zhang and Zhang (2018) showed the SST composites for QBOE minus QBOW in the Indian Ocean and west Pacific and indicated a possible relation to the Indian Ocean dipole. We note that a possible role for ENSO in the QBO–MJO relation is not in agreement with the findings of Nishimoto and Yoden (2017) and Son et al. (2017) that this link exists during DJF months that are in the neutral phase of ENSO. We examine *global* SST composites for QBOE and QBOW and show that the QBOE SST composite is remarkably similar to the La Niña composite.

We discuss two mechanisms by which the SST may modulate the QBO–MJO link during DJF. These are illustrated in Fig. 1. The first possibility, shown in Fig. 1a, is that the phase of the QBO is influenced by the phase of ENSO, and that the observed MJO power anomalies during DJF are actually produced by the SST anomalies associated with ENSO during DJF. The second possibility, shown in Fig. 1b, is that the QBO first influences the SST, possibly with an amplification due to the Bjerknes feedback, and the SST, in turn, affects the MJO. Our results are inconclusive, partially because our model, like others, is unable to successfully simulate the QBO–MJO link. Yet, we feel that the evidence we present is intriguing. Our work adds to the list of suggested mechanisms for the QBO–MJO connection, even if our idea, like others proposed previously, remains unproven at this point.

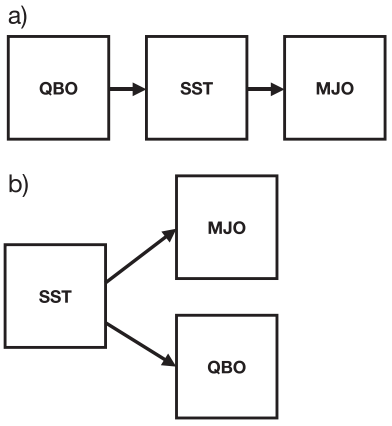

FIG. 1. An overview of the two mechanisms examined in the text by which the SST might affect the QBO–MJO connection.

2. Methods

a. Observations

We analyzed data from the ERA-Interim reanalysis of the European Centre for Medium-Range Weather Forecasts (years 1979–2014; Dee et al. 2011) for diagnosing stratospheric and tropospheric winds and SST. We use daily data for calculating the MJO power and monthly data for other purposes. Subsurface ocean temperatures along the equator are diagnosed using the Ocean Reanalysis Pilot 5 (ORAP5; Zuo et al. 2017). We also used the NOAA daily-mean outgoing longwave radiation (OLR; Schreck et al. 2018; Wang et al. 2021).

b. Simulations

We also analyzed simulations performed with a modified version of the Community Earth System Model (CESM), version 2 (Danabasoglu et al. 2020). The modified model, which we refer to as 83LCESM2, was developed by the CESM Vertical Grid Task Team. It uses the finite-volume dynamical core with a nominal 1° horizontal resolution and 83 layers, with its top at 0.008 hPa, and the physics from the Whole Atmosphere Community Climate Model, version 6 (WACCM6; Gettelman et al. 2019), with prescribed chemistry. The parameters for the convective gravity wave momentum transport parameterization were changed from those of the default WACCM6 physics package so as to obtain a realistic QBO.

Figure 2 shows model diagnostics of the MJO, QBO, and ENSO, based on a 98-yr coupled preindustrial simulation. Model 83LCESM2 produces a reasonable simulation of the MJO as evidenced in the Wheeler and Kiladis (1999) diagram shown in Fig. 2a. Figure 2b shows that the amplitude of the QBO variability calculated using Fourier decomposition following Dunkerton and Delisi (1985) is consistent with reanalysis. The Hovmöller plot

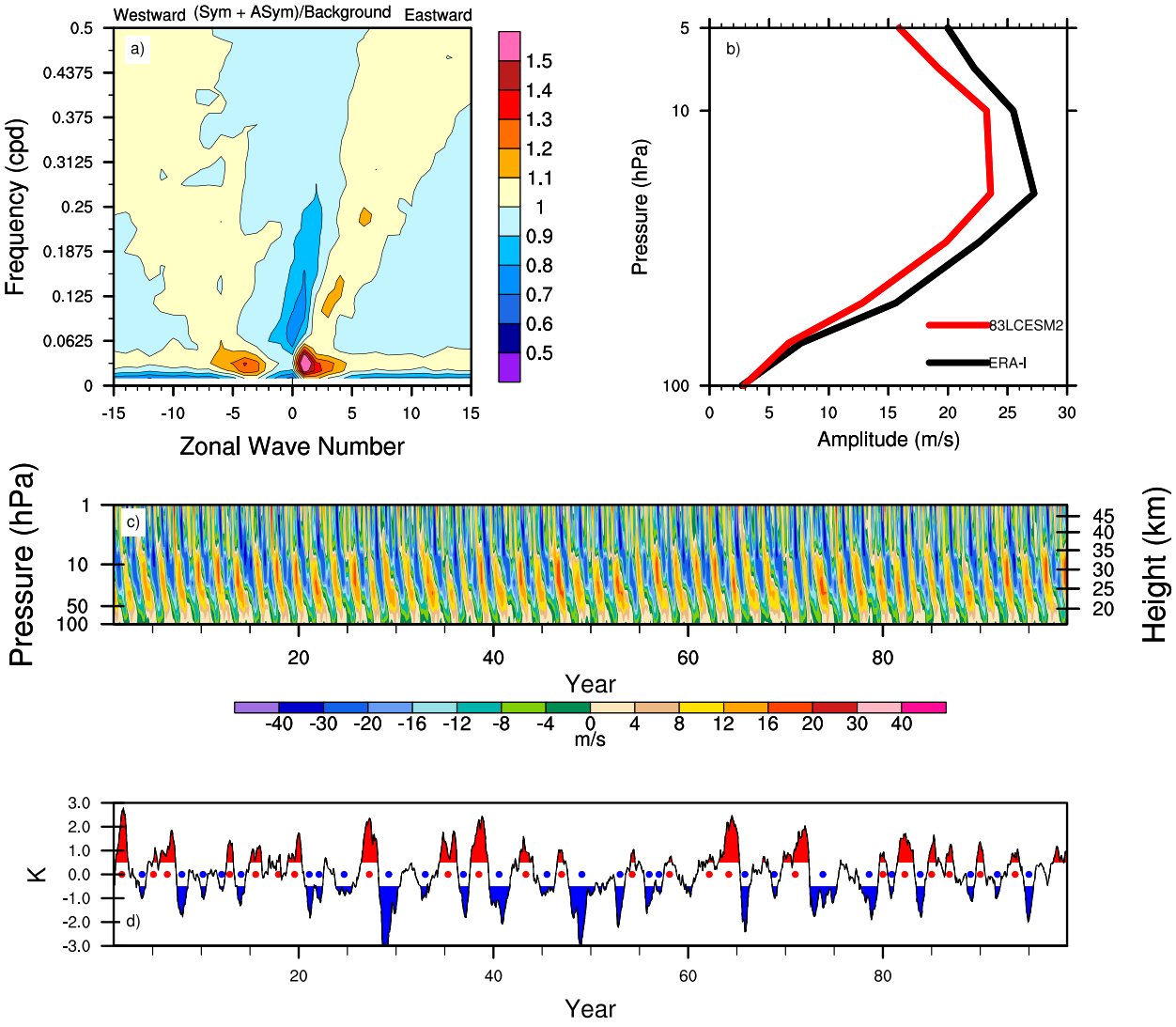

FIG. 2. The 83LCESM2 simulation of the MJO, QBO, and ENSO: (a) A Wheeler–Kiladis (zonal wavenumber–frequency normalized OLR power spectrum) diagram showing a somewhat realistic MJO signal. (b) The amplitude [i.e., Fourier amplitude, following Dunkerton and Delisi (1985)] of the QBO in meters per second as a function of pressure (hPa). (c) The zonal-mean zonal wind averaged between 5°S and 5°N. (d) The simulated Niño-3.4 SST time series, showing the ENSO signal. The red and blue dots mark the central months of the El Niño and La Niña events, respectively, used in the analysis described in the text.

shown in Fig. 2c shows a realistic QBO signal in the zonally averaged zonal velocity. The period of the QBO in this simulation is approximately 23 months, a little shorter than the average observed QBO period of 28 months. The simulated Niño-3.4 time series, shown in Fig. 2d, is somewhat realistic, but weaker than observed. Additional numerical experiments with specified SSTs are discussed later.

c. *QBOE and QBOW events*

Composite QBOs were constructed from the observed and simulated zonal wind data using the following procedure. First, the long-term mean, the secular trend, and the average seasonal cycle were removed from the data. The long-term mean and the seasonal cycle were removed by computing the long-term means for each of the 12 months and subtracting them from the corresponding monthly values for the individual years. Next, a bandpass Butterworth filter was applied, with cutoffs at 20 and 36 months. We will call this the QBO filter. We computed an area-weighted average of the filtered data over all longitudes and from 10°S to 10°N. The wind data as processed above, depend only on height and time and are referred to below as the "QBO-filtered zonal winds."

A given time is considered part of a QBOE event when the QBO-filtered zonal wind at 50 hPa is more negative than -5.0 m s^{-1}. For each string of one or more consecutive QBOE months, we identify the central month, which is assigned lag 0. The central month does not necessarily have the strongest signal and it does not need to be within DJF; it is

simply in the middle of the consecutive string. We then compute the mean over all QBOE events of the QBO-filtered zonal winds for lags of ±14 months relative to the central months. This yields a 29-month composite QBOE.

Similarly, a QBOW event occurs when the QBO-filtered zonal wind at 50 hPa is larger than 5.0 m s^{-1}. We follow the procedure described above to define QBOW events and composites relative to those events. Based on these criteria, the ERA-Interim record contains 10 QBOE events and 16 QBOW events. As mentioned above, the period of the QBO in the 98-yr simulation is approximately 23 months. We find that the simulation contains 30 QBOE events and 34 QBOW events.

We also composite the SST for performing atmosphere-only simulations with prescribed QBO SSTs. The SST composites for QBOE (or QBOW) are obtained by averaging over all Januaries, Februaries, and so on, that satisfy the QBOE (QBOW) criteria, creating a composite seasonal cycle for each event that is then prescribed in the model run.

d. El Niño and La Niña events and composites

To calculate the stratospheric (and tropospheric) zonally averaged zonal wind composites based on ENSO, the monthly mean SST was averaged for the Niño-3.4 region (5°S–5°N, 120°–170°W). Note that the Niño-3.4 SSTs have already been deseasonalized. El Niño months were defined as those for which the Niño-3.4 temperature anomaly exceeds 0.5 times the average standard deviation over the entire Niño-3.4 time series. Similarly, La Niña months were defined as those for which the Niño-3.4 temperature anomaly is more negative than −0.5 times the temporal standard deviation. Based on these criteria, the ERA-Interim record contains 10 El Niño events and 10 La Niña events, and the 98-yr simulation contains 22 El Niño events and 25 La Niña events.

A central month was chosen for each El Niño or La Niña event. The central month does not necessarily have the strongest signal. The mean zonal wind at various levels is composited for all central months chosen and assigned a lag 0. We similarly composite the zonal winds for each of the 14 months prior and the 14 months after each central month. The earlier and latter parts of 29-month composites for El Niño events may contain some signal of La Niña if the El Niño event is short.

We also composite the SST for performing atmosphere-only simulations with prescribed El Niño and La Niña SSTs. The SST composites for El Niño (or La Niña) are obtained by averaging over all Januaries, Februaries, and so on, that satisfy the El Niño (or La Niña) criteria, creating a composite seasonal cycle for each event that is then prescribed in the model run. In this way, we create composite SST seasonal cycles centered on El Niño and La Niña events.

e. A measure of MJO power

Following Kim et al. (2020), we calculated the DJF-averaged MJO power for each year as a function of longitude and latitude using the following procedure. We computed a measure of MJO power from the observed and simulated OLR data, following Wheeler and Kiladis (1999). The same procedures were used for the observations and simulations. The full time series were detrended, rather than 96-day overlapping segments as in Wheeler and Kiladis (1999). The monthly climatology (seasonal cycle) was removed by computing the long-term means for each of the 12 months and subtracting them from the corresponding monthly values for the individual years. Five percent of the data were tapered to zero at the ends of the time series to minimize spectral leakage. After tapering, a complex fast Fourier transform was performed, and the wavenumber–frequency data were filtered to retain only the eastward propagating coefficients for 20–100-day periods and wavenumbers 1–5. We refer to the result as the MJO-filtered OLR. The MJO power at a given grid point is then defined as the standard deviation (not the variance) of the MJO-filtered OLR across all December–February (DJF) days that fall into a particular category, e.g., DJF days for all years, DJF days for QBOE years, or DJF days for QBOW years.

f. Maximum covariance analysis (MCA)

We use MCA to analyze the covariance of the monthly SST and the MJO power. While principal component analysis (also known as empirical orthogonal functions) analyzes the modes of variability of a single field (say monthly SST), MCA examines the covariance between two different fields, in our case, the monthly SST and the MJO power during DJF only. The analysis proceeds by first placing the data from all M SST grid points and N DJF months into an $M \times N$ data matrix $\mathbf{T}$ whose columns are the monthly values of the SST, and the MJO power from L grid points into a second $L \times N$ matrix $\mathbf{P}$. The $M \times L$ covariance matrix of the two fields is calculated as $\mathbf{C} = \mathbf{T}\mathbf{P}^{\mathrm{T}}/N$. Then, the singular value decomposition (SVD) of the covariance matrix, $\mathbf{C} = \mathbf{U}\mathbf{\Sigma}\mathbf{V}^{\mathrm{T}}$ is calculated. The columns of $\mathbf{U}$ and $\mathbf{V}$ represent the spatial patterns of the covariability between the two fields. In particular, the first $\mathbf{U}$ vector shows the spatial pattern of SST correlated with the spatial pattern of MJO power shown by the first $\mathbf{V}$ vector, and these two first vectors represent the most correlated patterns of the two fields. The singular values in $\mathbf{\Sigma}$ provide information about the percentage of *covariance* explained by each pair of $\mathbf{U}$, $\mathbf{V}$ vectors, and one can also find out how much of the *variance* of each field is explained by each of these vectors (Bretherton et al. 1992).

To determine the statistical significance of the difference in MJO power between QBOE and QBOW, we used a bootstrapping method as follows. As mentioned above, there are 10 QBOE years and 16 QBOW years in the 35-yr record. We randomly sample 26 (=10 + 16) years of DJF data, allowing a given year to be sampled more than once (i.e., sampling with replacement). The first 16 years were arbitrarily denoted as "QBOW" and the remaining ten as "QBOE." The MJO power was computed for the "QBOE" and "QBOW" DJFs at each longitude and latitude. This random sampling procedure was repeated 1000 times to obtain a set of MJO power with random QBO phases. To measure the statistical significance, we computed the 10th and 90th percentile of the 1000 samples, and stippled areas where the MJO power difference is positive and above the 90th percentile of the 1000 samples, or negative and smaller than the 10th percentile. This bootstrapping test was

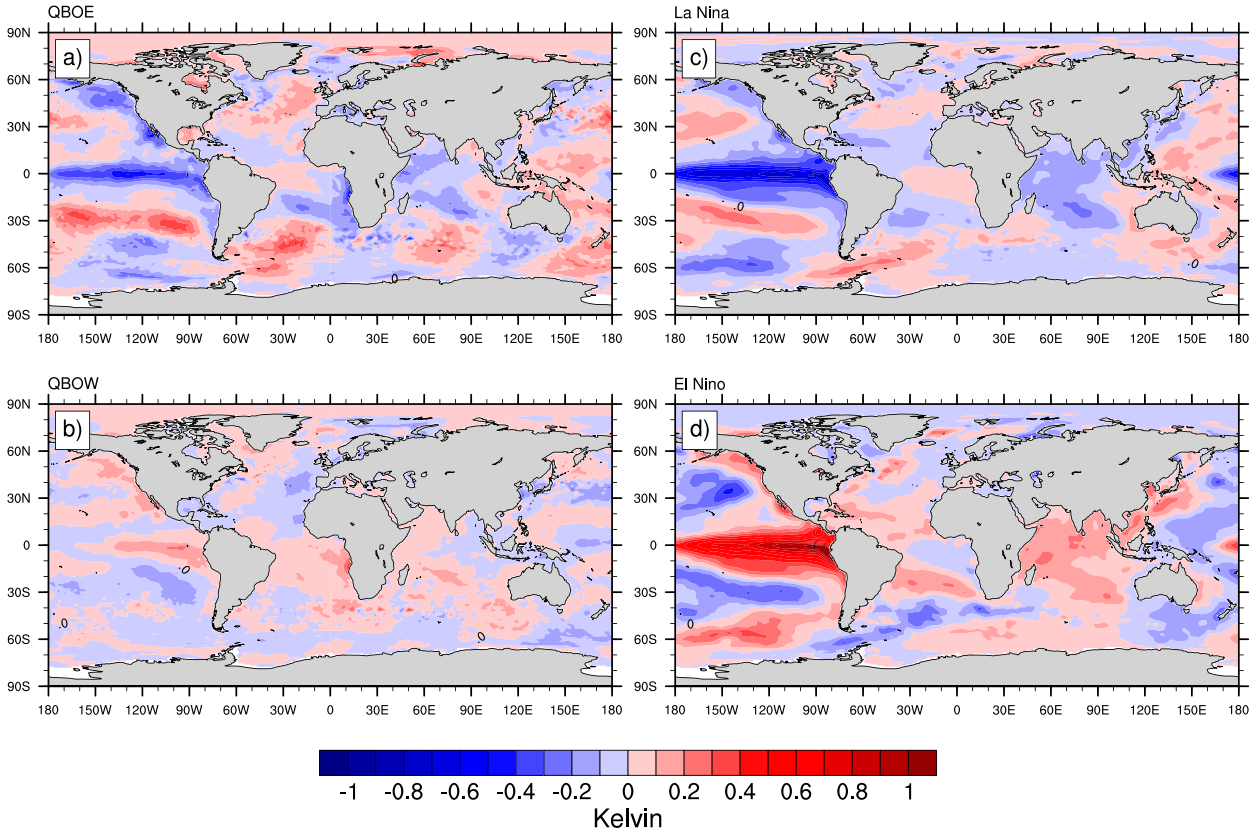

FIG. 3. (a) Observed global QBOE SST anomalies relative to climatology, (b) observed QBOW SST anomalies relative to climatology, (c) observed global La Niña SST anomalies relative to climatology, and (d) observed global El Niño SST anomalies relative to climatology. All panels are based on DJF data only.

applied to both the simulations and observations. A very similar bootstrapping method is used to determine the statistical significance of the difference in MJO power between El Niño and La Niña events.

3. Results

a. *Observations*

To explore the possible role of the SST in coupling the QBO and the MJO, we constructed global composite SST anomalies for QBOE and QBOW events. The anomalies are computed relative to the mean over the entire dataset. Figures 3a and 3b show the anomalies for QBOE and QBOW events using only DJF data. The corresponding anomalies for El Niño and La Niña are shown in Figs. 3c and 3d. There is a remarkable similarity between the SST composites for QBOE and La Niña (cf. Figs. 3a,c). The patterns resemble each other even in areas far outside the Equatorial Pacific, including the mid- and high-latitude Pacific, as well as the Atlantic and Indian Oceans; the *global* spatial correlation is 0.66. In contrast, there is much less similarity between the SST composites for QBOW and El Niño (cf. Figs. 3b,d), which have a global pattern correlation of only 0.22. The El Niño anomaly is nearly 180° out of phase with the La Niña anomaly, but the QBOW anomaly does not resemble minus the QBOE anomaly. The QBOW anomaly only slightly resembles the El Niño anomaly. Among the 10 QBOE DJF events, seven occur when Niño-3.4 index is negative, while only three occur during the positive ENSO phase. Although not all strong La Niña events coincide with QBOE events, it does seem that, when La Niña and QBOE happen together, the La Niña is particularly strong (not shown), suggesting a QBOE–La Niña link. See Zhang and Zhang (2018) for a closely related analysis.

Figures 4a and 4b show the DJF MJO power averaged over the QBOE and QBOW events from reanalysis, and Fig. 4c shows the difference between the two. The results are consistent with Yoo and Son (2016), showing more MJO power during QBOE, and less power during QBOW. The existence of a clear QBOE SST signal and its similarity to the La Niña SST signal suggests that the MJO power difference between QBOE and QBOW may, in fact, be driven by SST differences. Possible mechanisms for the QBOE and QBOW SST differences are discussed below.

We next used a maximum covariance analysis (Bretherton et al. 1992) to quantify the connection between the SST and the MJO power, as explained in section 2f. We first apply a Butterworth filter to both the MJO power and the SST, to focus on the ENSO signal, with periods in the range of 36–60 months. We call this the ENSO filter. Figures 5a and 5b show the MCA results. Figure 5a shows the first SVD vector

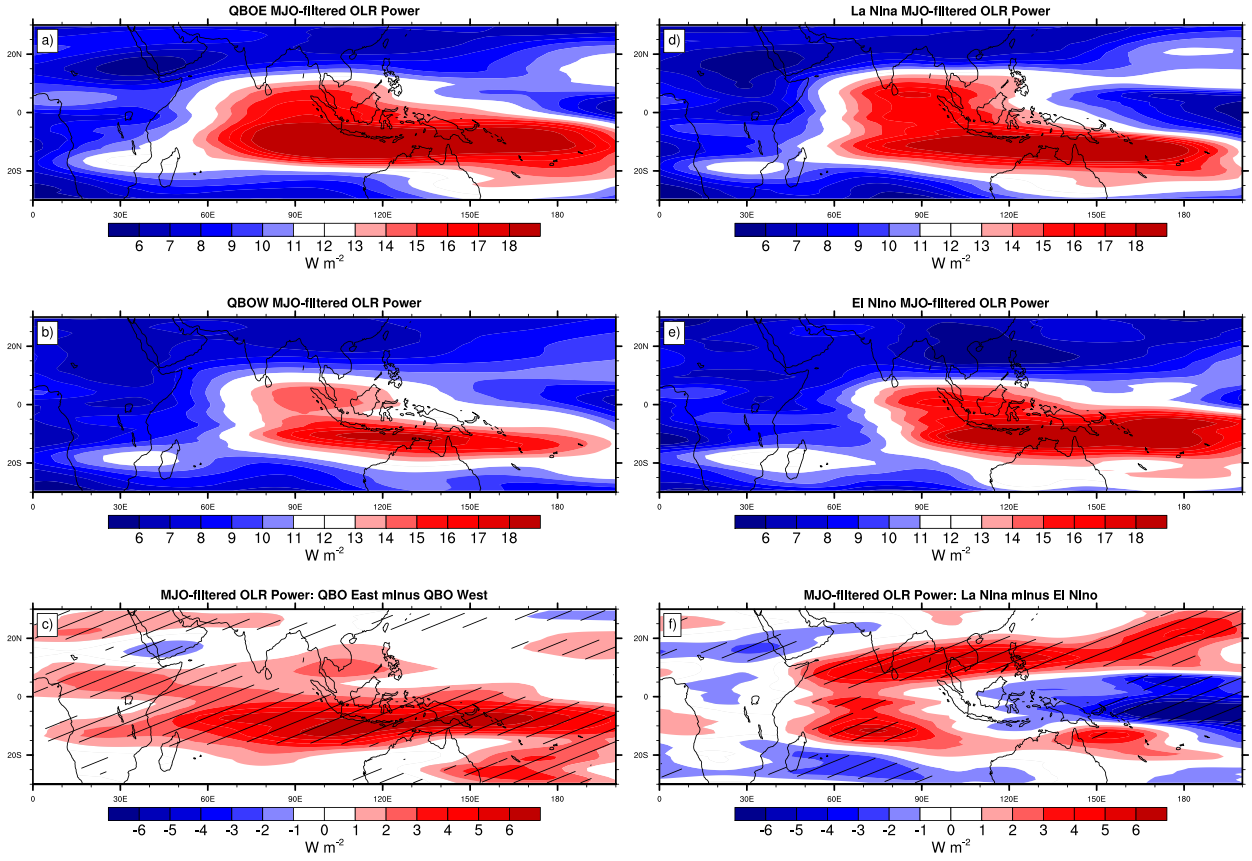

FIG. 4. Observed MJO power for QBO and ENSO years: Observed (a) QBOE and (b) QBOW DJF MJO power (section 2). (c) The difference of (a) − (b). (d) La Niña and (e) El Niño MJO power (composite restricted to DJF and based on Niño-3.4). (f) The difference of (d) − (e). Hatching shows statistical significance (above 90%) based on bootstrapping, as described in the text.

corresponding to the SST, which is characterized by an east–west dipole structure in the west Pacific and Indian Ocean, and strong La Niña–like SST cold tongue along the equator to the east. The SST signal in the Indian Ocean is reminiscent of the Indian Ocean dipole (Saji et al. 1999) that is likely at least partially correlated with ENSO (Zhao and Nigam 2015). Figure 5b shows that the corresponding ENSO-filtered MJO power first SVD mode shows reduced MJO power over the so-called Maritime Continent. Both the SST and MJO power structures in Figs. 5a and 5b are consistent with those of La Niña minus El Niño shown in Figs. 3c and 4f, respectively. These leading MCA modes explain 74% of the covariance between the MJO power and SST filtered fields, as well as 54% of the variance of the SST and 18% of the variance of the MJO power. The significant percentages of both covariance and variance explained by the first SVD mode suggest a nonnegligible connection between the MJO power and the SST when both are ENSO-filtered. The MCA analysis thus confirms that there is a connection between SST and MJO power on ENSO time scales, as previously discussed by Tang and Yu (2008), Chen et al. (2015), Schirber (2015), Pang et al. (2016), Wang et al. (2018), Sun et al. (2019), and Hendon et al. (1999).

Figures 5c and 5d show the corresponding results when the QBO filter is used. The east–west SST dipole pattern is similar to that on ENSO time scales except in the east Indian Ocean and around the Maritime Continent (cf. Figs. 5a,c). The corresponding MJO power patterns on ENSO and QBO time scales are different (Figs. 5b,d). The MCA pattern of the MJO power on QBO time scales (Fig. 5d) shows an overall positive anomaly over much of the Indian Ocean, although it is close to zero over the Maritime Continent. This pattern is reminiscent of the MJO power composite for QBOE minus QBOW that one would want to explain (again, precluding the Maritime Continent, Fig. 4c), supporting a possible role for the SST. In this case, the leading MCA mode explains 60% of the covariance between the two fields, indicating that it accounts for much of the QBO–SST connection on QBO time scales as well. The SST pattern also explains 46% of the variance of the SST itself. The large fraction of SST variability explained by the SST SVD models on both ENSO and QBO time scales is likely due to the fact that these SST patterns are similar to those of ENSO, which is known to account for a large part of the SST variance. Last, 24% of the variance of the QBO-filtered MJO power is explained by the pattern that is involved in the covariance with the SST, again a nonnegligible part of the MJO power variability. For completeness, Figs. 5e and 5f show the same analysis without filtering, i.e., including all time scales.

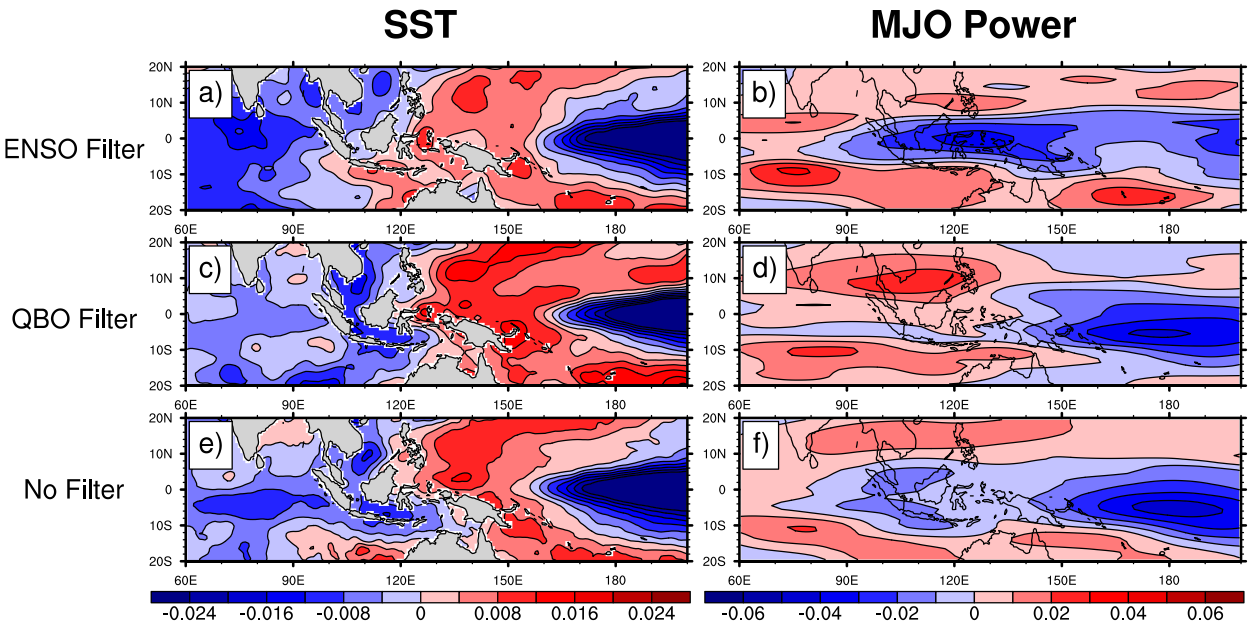

FIG. 5. Maximum covariance analysis of SST and MJO power: (a) The first SST SVD mode pattern (nondimensional), calculated based on ENSO-filtered SST (Butterworth-filtered with cutoffs of 36 and 60 months). (b) The first MJO power SVD mode pattern, with variance based on an ENSO time scale in the range of 36–60 months. (c) The first SST SVD mode based on the QBO-filtered SST (Butterworth of 20–36 months). (d) The first MJO power SVD mode pattern, based on a QBO time scale in the range of 20–36 months. (e),(f) The same results with no filtering.

Note the differences in the patterns between Figs. 4b and 3f, where the longitude of the maximum negative signal is different. One expects these analyses to be similar, as both look at the relation between SST and MJO power, and indeed the patterns are related. However, Fig. 3f shows the effects of ENSO SST specifically, while Fig. 4b shows the general relation between SST and MJO power: hence, the difference.

Overall, the MCA analysis suggests that MJO power and SST are strongly linked on the ENSO time scale, as also pointed out by the earlier works cited above. More relevant to our purpose here, we also note that MJO power and SST are strongly linked on the QBO time scale, a connection that, as far as we know, has not been discussed previously. This MJO–SST link on the QBO time scale, which is the focus of this paper, may be part of the mechanism that gives rise to the QBO–MJO connection. The above composite and MCA analyses are not conclusive due to the short and noisy observed record, but they do strongly suggest a role for the SST. The correlations that we have identified do not imply causality and do not address the mechanism through which the SST affects the MJO power. We attempt to address these issues further through the simulations discussed below.

b. *Simulations*

We used 83LCESM2 (see section 2) to further study the role of the SST in mediating the QBO–MJO power connection. The results are shown in Fig. 6, which should be compared with Fig. 4. The simulated MJO power is strongest over the central Indian Ocean, while in observations the maximum power region extends all the way from the central Indian Ocean to east of the Maritime Continent. We return to this difference below. Figure 6c shows that the coupled model simulates a very weak MJO power signal for the difference of QBOE minus QBOW over the Maritime Continent and the Indian Ocean. These simulated signals do not agree with the observed signals shown in Fig. 4c). We thus find ourselves in a position similar to that of previous authors who struggled to study the observed QBO–MJO connection with similar global models (Lee and Klingaman 2018; Lim and Son 2020; Kim et al. 2020; Martin et al. 2021c).

Figure 7 shows the QBO and ENSO SST anomalies for DJF, as simulated by the coupled model, for comparison with the observations shown in Fig. 4. The simulated La Niña and El Niño signals are strong. They also show an Indian Ocean signal that projects on the Indian Ocean dipole pattern (Saji et al. 1999), and we discuss below a possible role for the Indian Ocean thermocline depth and its feedback on the SST. The simulated SST anomalies for QBOE and QBOW are significantly weaker than observed. There is a weak negative SST signal in the central equatorial Pacific for QBOE (Fig. 7a) that is of the same sign as the simulated La Niña SST anomaly. The global pattern correlation between Figs. 7a and 7c is 0.24. While it is disappointing that the model does not simulate the observed QBO–MJO connection, the fact that it also does not show the strong observed SST signal of QBOE is at least consistent with our hypothesized role for the SST in bringing about the observed QBO–MJO connection. In other words, it is possible that the model fails to simulate the observed QBO–MJO connection *because* it fails to simulate the observed SST signal of QBOE.

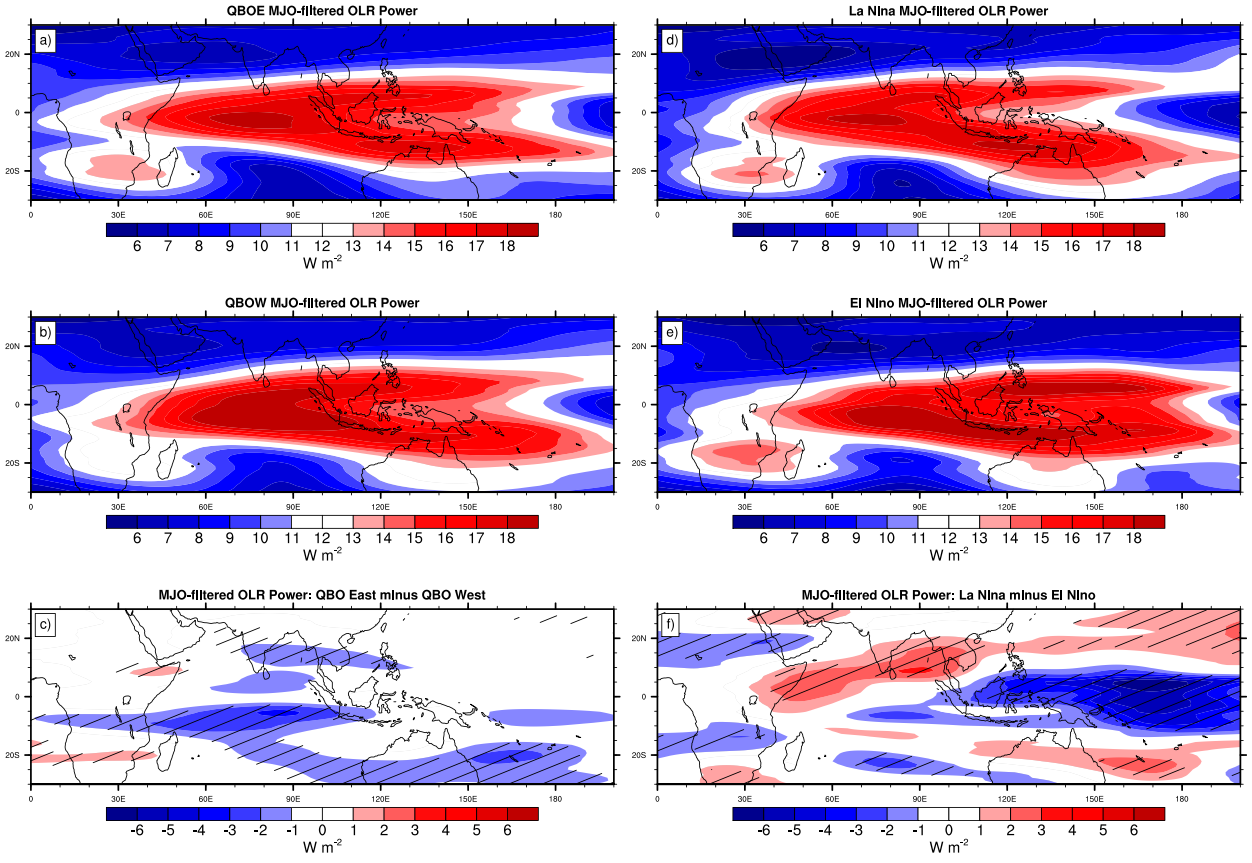

FIG. 6. As in Fig. 4, but for the coupled 83LCESM2 simulation.

To further investigate this possibility, we performed experiments using 83LCESM2 with prescribed SSTs, using several prescribed seasonally varying monthly SST datasets, which were created by compositing the ERA-Interim SSTs. We performed two 10-yr simulations driven with the prescribed SSTs for QBOE and QBOW (see section 2c). We also performed two longer, 20-yr simulations, required due to the longer ENSO time scale, driven with the SSTs composited over the observed La Niña and El Niño events (see section 2d). The overall MJO power in these uncoupled simulations (not shown) is much weaker than in the coupled simulation discussed earlier, as has been found in previous studies of uncoupled atmospheric models with prescribed SSTs (e.g., Woolnough et al. 2007).

For ease of comparison with the observations and the results from the coupled model, Figs. 8a and 8d are repeated from Fig. 4, and Figs. 8b and 8e are repeated from Fig. 6. Figure 8c shows the difference in MJO power between the uncoupled QBOE and QBOW simulations. The model produces a modest enhancement of MJO power with prescribed QBOE SSTs, relative to prescribed QBOW SSTs.

The simulated enhancement of the MJO power during QBOE, as seen in Fig. 8c), is strongest near the Maritime Continent, and does not extend as far west as the observed enhancement (cf. Figs. 8a and 4c). The amplitude of the simulated enhancement is also weaker than observed. Nevertheless, the results with the specified SST anomalies are much more realistic than those from the coupled model (Fig. 8b).

In Figs. 8a–c, the annual-mean background MJO power is shown using contours. The enhanced QBOE power shown in Fig. 8a (the observations) and Fig. 8c (the uncoupled model) are approximately collocated with the annual-mean background MJO power, so the errors in the location of the MJO power enhancement shown in Fig. 8c may stem from errors in the location of the background power.

The results shown in Fig. 8 suggest that the SSTs produced in the coupled simulation contribute to and perhaps even explain the failure of the coupled simulation to reproduce the observed QBO–MJO connection. It is consistent with our hypothesis that the influence of the QBO on the SST leads to the observed MJO power differences between QBOE and QBOW. The inability of the coupled model to simulate the QBO–MJO connection could imply that the simulated SST does not respond to the QBO. We will discuss possible mechanisms later in this paper.

Figure 8f shows the MJO power difference between an uncoupled model run with prescribed observed composited La Niña SSTs and a corresponding run with prescribed observed composited El Niño SSTs. The simulated MJO power difference between these uncoupled simulations is similar to both

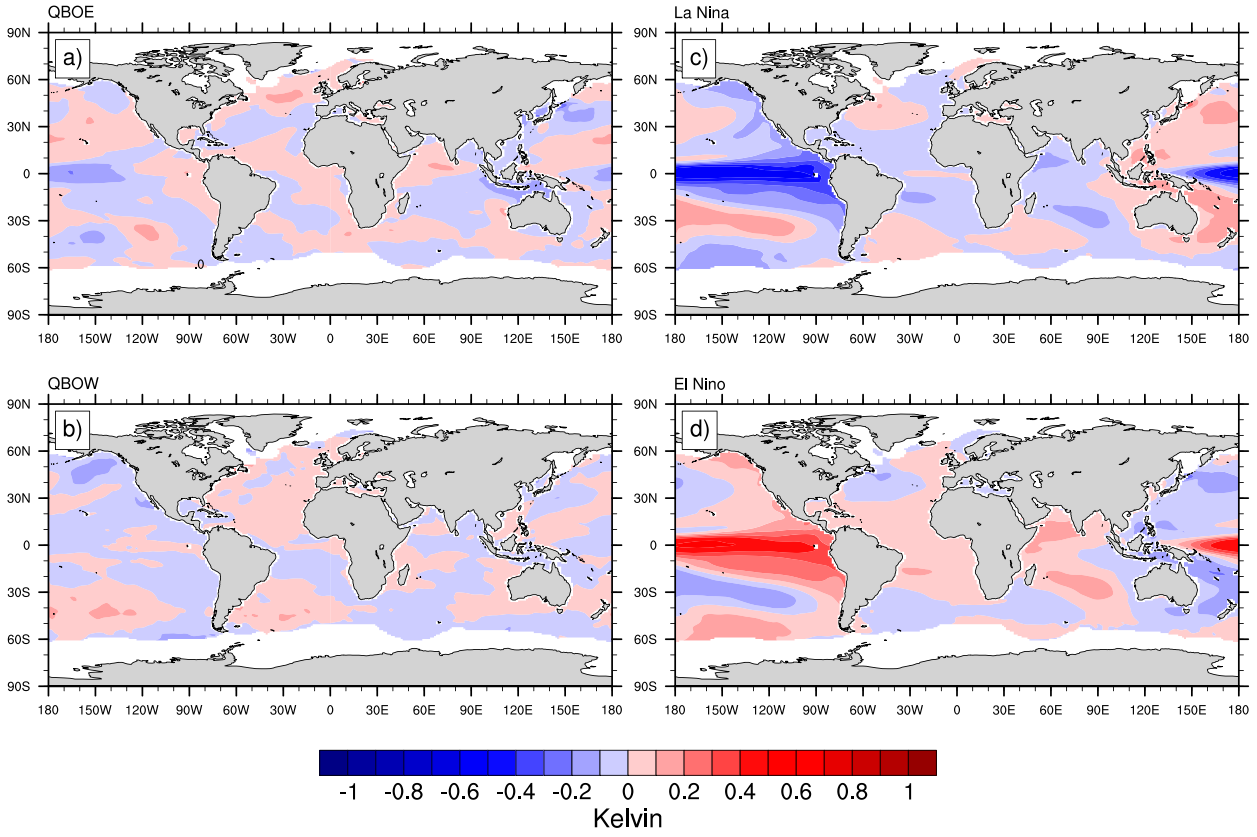

FIG. 7. Coupled 83L model SST composites for QBO and ENSO: (a) global QBOE SST, (b) QBOW SST, (c) La Niña SST, and (d) El Niño SST. All panels use DJF data only.

the observed difference as shown in Fig. 8b) and the difference simulated by the coupled model as shown in Fig. 8e). These similarities suggest that 1) the MJO power variations due to ENSO are likely driven by the SST differences between El Niño and La Niña, and 2) the model is able to reproduce this effect of the SST on the MJO power on ENSO time scales. This is supported by the fact that the spatial correlation between the coupled model's MJO power response to ENSO in Fig. 6f and the corresponding observed response in Fig. 4f is very high, 0.64.

c. *Further analysis*

Returning to the connection between ENSO and the QBO (Taguchi 2010), Fig. 9 shows Hovmöller diagrams for the observed QBO-filtered zonal winds composited for La Niña (Fig. 9a) and El Niño (Fig. 9c) events (section 2d). Figure 10 shows the corresponding diagrams based on the 98-yr coupled simulation. In each figure, panels b and d show the corresponding composites for QBOE and QBOW events, respectively; these are provided mainly for comparison with the La Niña and El Niño composites in panels a and c, respectively. All of the composites are plotted from 14 months prior to the central month to 14 months after. A bootstrapping method was used to determine statistical significance, which is indicated by stippling in Figs. 9 and 10.

In agreement with Kiladis et al. (2001), Schirber (2015), Geller et al. (2016), and Christiansen et al. (2016), there is a clear QBO signal in Figs. 9a and 9c, showing that in the real world there is a strong link between ENSO and the QBO. The downward propagation is faster for El Niño and slower for La Niña (Geller et al. 2016). The phase of the El Niño composite (Fig. 9c) is similar to the phase of the QBOW composite (Fig. 9d), but the La Niña composite (Fig. 9a) is nearly 180° out of phase with the QBOE composite (Fig. 9b). This is surprising given the similarity between the SST signals of La Niña and QBOE (Fig. 3), and it suggests that the QBO is driven by an atmospheric process associated with ENSO (e.g., convection) that is related to the SST in a more complex way (Taguchi 2010; Yuan et al. 2014). Figure 9 also shows a statistically significant signal in the tropospheric zonal wind for QBOE, but not for QBOW.

Figures 10a and 10b, corresponding to the La Niña and QBOE signals, are similar to the corresponding panels of Fig. 9. Figure 9c (for El Niño) shows a well-defined QBO signal, but Figs. 9c and 10c are not similar. While the reanalysis shows a strong stratospheric zonal wind signal for El Niño/La Niña (cf. Figs. 9a,c), the model shows a well-defined signal for La Niña and essentially no signal for El Niño (cf. Figs. 10a,c). This difference between the observations and the model suggests again that the model cannot realistically simulate an interaction between the

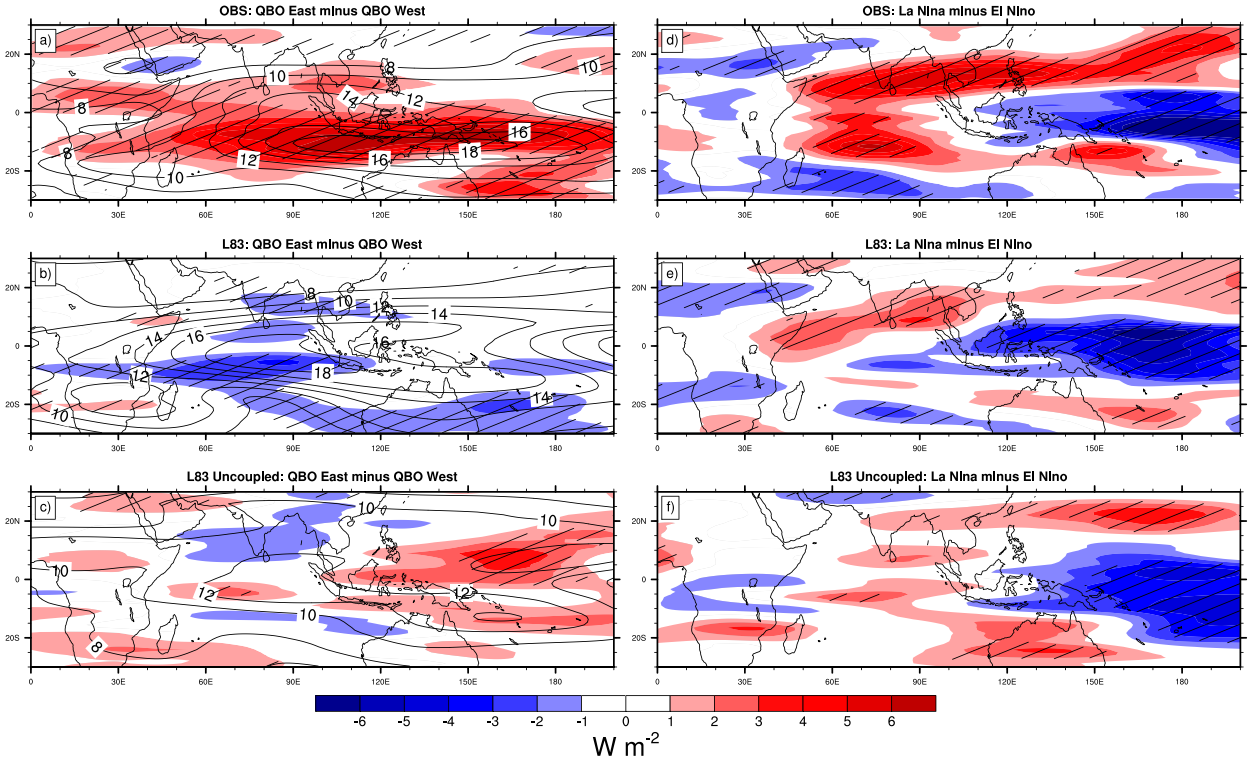

FIG. 8. MJO power differences for DJF: (a),(d) Repeated from Fig. 4. (b),(e) Repeated from Fig. 6. (c) The simulated MJO power difference between an uncoupled model run with prescribed observed composited QBOE SSTs and a corresponding run with a prescribed composited QBOW SSTs. (f) The MJO power difference between an uncoupled model run with prescribed observed composited La Niña SSTs and a corresponding run with prescribed observed composited El Niño Niño SSTs. In (a)–(c), the annual-mean background MJO power is shown using contours.

QBO and MJO that is modulated by the SST and ENSO, if indeed such a modulation exists, as suggested by the observations. Specific model deficiencies that may play a role in this failure include inaccuracies in the simulation of ENSO and the shorter-than-observed QBO period.

We next examine the possibility that the QBO wind signal reaches the surface and affects the SST. The observed Hovmöller diagrams in Fig. 9c show the propagation of QBO zonal wind anomalies all the way from the upper stratosphere to the surface. This surface zonal wind signal of the QBO is consistent with the analysis of Gray et al. (2018), who show in their Fig. 5 the results of a regression between the QBO signal and surface zonally averaged zonal winds. They also discuss a tropical mechanism for QBO influence at the Earth's surface (their Fig. 1). The propagation of the QBO signal to the surface seen in the above observational analysis is not seen in the coupled model results (Fig. 10c). This is consistent with our hypothesis that the failure of the SST to respond to the QBO in the coupled model is the reason for the coupled model being unable to reproduce the mechanism sketched in Fig. 1a for the QBO–MJO connection.

The composited Hovmöller diagrams of the zonal wind based on ENSO as well as that based on the QBOE/QBOW (Fig. 9) hint at a tropospheric signal, although it is difficult to see because it is much smaller than the stratospheric signal. It is easier to see a QBO signal at the surface using the regression analysis shown in Fig. 11. Figure 11a shows the observed time series of the 50-hPa zonally averaged zonal wind (blue curve; left scale) and the 10-m zonal wind averaged between 5°S and 5°N and over the longitudes between 60°E and 180° (red curve; right scale). Both time series have been QBO filtered. Figure 11b shows the lagged correlation of the two time series shown in Fig. 11a. A positive lag here means that the 50-hPa zonally averaged zonal wind leads. The figure shows that the two time series have a significant maximum correlation of slightly less than 0.4 in absolute value, with the 50-hPa zonally averaged zonal wind leading by 4 months. The correlation at zero lag is negative. The QBO-filtered surface wind signal has an amplitude of about 0.4 m s^{-1}. While not large, this is a non-negligible signal relative to, say, the corresponding ENSO variations, especially given that it is averaged over a wide range of longitudes. We speculate that this near-surface wind signal that is correlated with the QBO may be amplified by the Bjerknes feedback and contributes to the SST variability, as discussed below. The correlation between the QBO and the surface wind without the QBO filtering is, not surprisingly, much weaker (dashed line in Fig. 11b), but it is not completely negligible. We note that the correlation analysis of Son et al. (2017) between the MJO power and *U* at 50 hPa (U50) is based on DJF MJO power only, whereas our correlation analysis of U50 versus *U* at

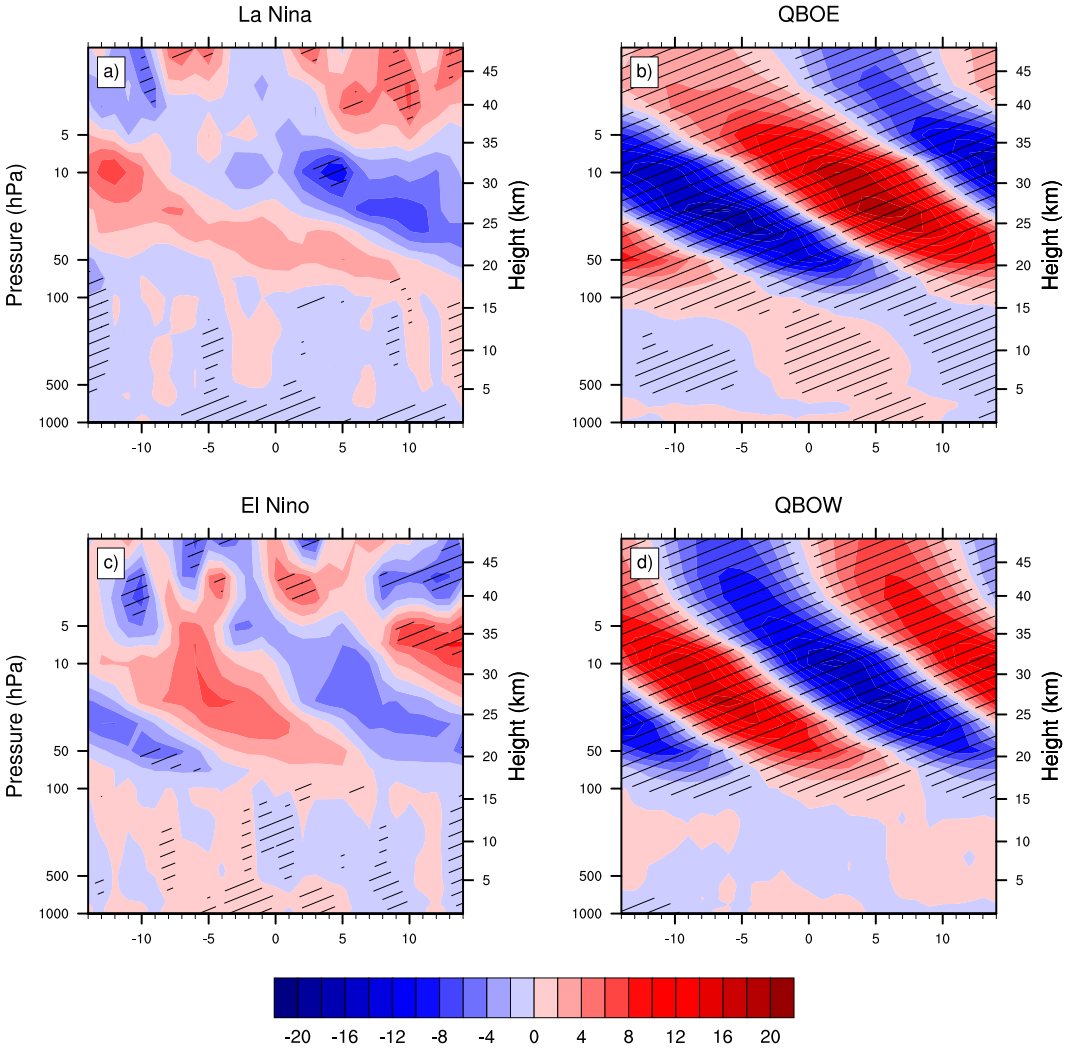

FIG. 9. Observed composite Hovmöller diagrams for the zonally averaged zonal wind, averaged from 10°S to 10°N as a function of time and pressure: (a) La Niña, (b) QBOE, (c) El Niño, and (d) QBOW.

10 m is based on all months. We chose to use all months because our goal is to identify a QBO signal at the surface that can influence the SST, and such a signal need not be limited to DJF.

The subsurface ocean temperature composites in Fig. 12 are relevant to the possibility that the QBO affects the SST. The figure shows the subsurface ocean temperature anomalies based on composites for both phases of the QBO (Figs. 12d,e) and ENSO (Figs. 12a,b) and the differences (Figs. 12c,f). There is a similarity between the western Pacific and Indian Ocean subsurface signal between La Niña and QBOE, although the western Indian Ocean and eastern Pacific signals are different. The QBOE–QBOW and La Niña minus El Niño signals are also quite similar. The similarity is seen in both the Pacific and the Indian oceans. The temperature anomalies are mostly strongest near the thermocline depth, at about 100 m. It is possible for these subsurface signals to affect the SST through upper-ocean mixing, as occurs as part of the ENSO cycle in the east Pacific and as seems to be the case in these composites. Once the SST responds to the thermocline change, the surface winds may further respond to that, and such feedback may account for some of the surface wind signal seen in Fig. 11b. Feedbacks between the SST, thermocline depth and surface winds may then further amplify the SST signal over both the western Pacific and the Indian Ocean, similar to the Bjerknes feedback in the equatorial Pacific (Bjerknes 1969). On the other hand, the SST/thermocline feedback shown in Fig. 12 may be the response of the Indian Ocean dipole (Saji et al. 1999) to ENSO (Zhao and Nigam 2015) rather than to a surface wind signal that is associated with the QBO as speculated here.

4. Conclusions

Previous studies have identified a QBO–MJO connection, in which MJO power is enhanced when the QBO is in its easterly phase during the northern winter months (Yoo and Son 2016; Zhang and Zhang 2018; Nishimoto and Yoden 2017;

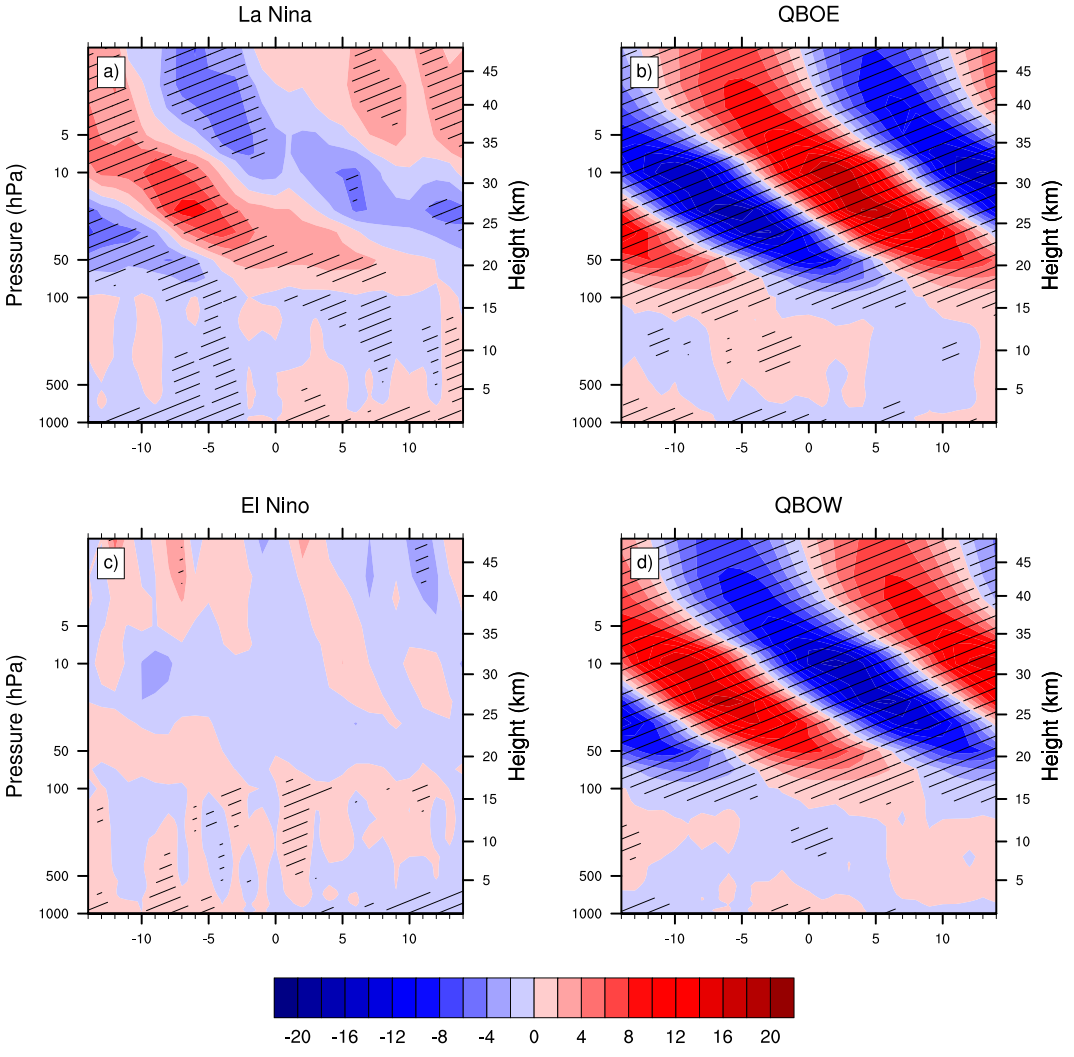

FIG. 10. As in Fig. 9, but simulated.

Marshall et al. 2017; Son et al. 2017; Martin et al. 2021c). Several mechanisms have been suggested, but none have been conclusively supported using observations or simulations (Martin et al. 2021c,a).

Our objective in this study has been to examine the hypothesis that the QBO–MJO connection is modulated or facilitated by changes in the SST pattern, and perhaps specifically by ENSO. Two possibilities are schematically depicted in Fig. 1. We used reanalysis and numerical simulations to examine various aspects of this hypothesis.

We began by pointing out a remarkable similarity between the *global* SST composited on QBOE and the corresponding global SST composite for La Niña events. This similarity extends far beyond the tropics. It suggests that La Niña and QBOE are partially synchronized, in the sense that they tend to occur during the same months. A possible connection between the SST in the west Pacific and Indian Ocean and the MJO on QBO time scales was previously discussed by Zhang and Zhang (2018), who suggested a role for the Indian Ocean dipole. Using maximum covariance analysis, we found a covariability of the MJO power and SST in the tropical Indian Ocean and western Pacific. Together with the SST similarity between QBOE and La Niña, this lends support to our hypothesis that the SST plays a role in the QBO–MJO connection. In our study, we examined this possibility and several mechanisms by which it may be realized.

The similarity of the SST composites during QBOE and La Niña suggests that what seems to be an effect of the QBO on MJO power may actually be a result of the SST influencing both the QBO and the MJO (Fig. 1b). With this in mind, we began by exploring the role of ENSO, while still recognizing that the SST might facilitate the QBO–MJO connection without involving ENSO. We examined the possibility that ENSO is driving the QBO, or is synchronized with it (Taguchi 2010; Yuan et al. 2014; Schirber 2015; Geller et al. 2016; Christiansen et al. 2016), and that ENSO's SST signal then also affects the MJO power, in such a way that the MJO power and the phase of the QBO are correlated with each other (Fig. 1b). As a first step, we identified a connection between ENSO and the QBO

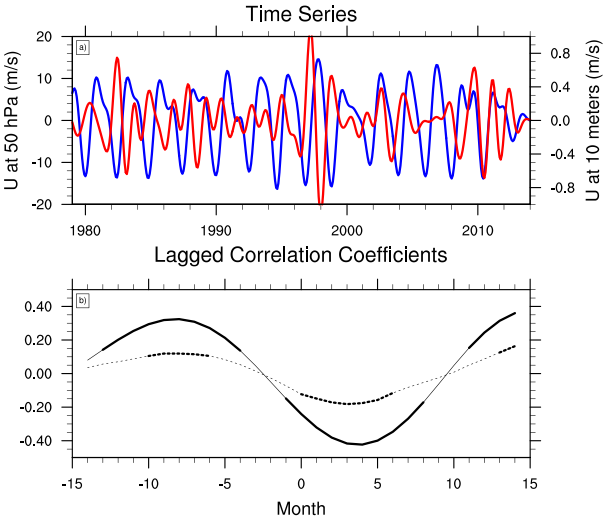

FIG. 11. (a) Observed time series of the 50-hPa zonally averaged zonal wind (blue curve; left scale) and the 10-m zonal wind between 5°S and 5°N, averaged over the longitudes between 60°E and 180° (red curve; right scale). Both time series have been QBO-filtered. (b) The lagged correlation of the two time series that are shown in (a). The solid curve corresponds to the QBO-filtered time series, and the dashed curve is based on the unfiltered time series. A positive lag means that the 50-hPa zonally averaged zonal wind leads the 10-m zonal wind. Thick segments are statistically significant with $p < 0.05$.

in the zonally averaged lower stratospheric zonal wind composited for La Niña and El Niño events, in line with previous studies (Taguchi 2010; Schirber 2015; Geller et al. 2016; Christiansen et al. 2016). Next, compositing the MJO power over the Maritime Continent and the Indian Ocean based on the phase of ENSO phase shows that the MJO is stronger during La Niña events.

From a physical mechanism point of view, ENSO may regulate the phase of the QBO, through changes in the vertical wave transport of westerly momentum (Taguchi 2010; Yuan et al. 2014; Geller et al. 2016). And, of course, the MJO power may be affected by the ENSO SST (Tang and Yu 2008; Chen et al. 2015; Pang et al. 2016; Wang et al. 2018; Sun et al. 2019). It is, therefore, not impossible to imagine the QBO–MJO connection as the result of both the MJO and QBO being affected by the ENSO SST. The lack of similarity between the responses of the MJO power to ENSO and the QBO may indicate that the small differences between the ENSO and QBO SST composites are significant as far as driving the MJO power signal is concerned. It is possible that the link involves only eastern Pacific or only central Pacific ENSO events, for example, and this could be an interesting direction for future explorations. However, the short observational record implies that such an exploration would need to be based on a model that successfully simulates the QBO–MJO connection and can be run for longer times. Previous studies (Garfinkel and Hartmann 2007) found that the correlation between the QBO and ENSO is nonstationary, negative in the first part of the record and positive later, and overall weak (Hu et al. 2012). It seems that this does not preclude the QBOE–La Niña connection we find here, and one might conclude that the possible role of the SST and ENSO does not apply symmetrically to both El Niño and La Niña SSTs, although a potential link of the QBO to *strong* El Niño events has also been suggested (Christiansen et al. 2016).

We now turn to the possibility that the QBO drives SST anomalies that then affect the MJO, as schematically depicted in Fig. 1a). One way that this could work is through QBO-induced effects on cloud cover (Sweeney et al. 2023), which could then influence the SST through changes in shortwave radiation. We do not explore this possibility here. We do discuss a second possible mechanism for an effect of the QBO on the SST: we found that QBO zonal wind anomalies propagate all the way from 50 hPa to the surface (Fig. 9b); this result is supported by an (admittedly weak) correlation between the QBO and surface winds (Fig. 11). The penetration of the QBO signal into the troposphere supports the possibility that the SST may be directly affected by the QBO, even without the involvement of ENSO. This is consistent with the connection between the QBO and surface winds discussed by Gray et al. (2018). The idea is further supported by our finding that there is a significant QBO signal in composites of subsurface thermocline-level ocean temperatures along the equator in the Indian and west Pacific oceans Fig. 12. This subsurface temperature signal suggests a Bjerknes feedback between the ocean and the surface wind that is triggered by and amplifies a QBO surface wind signal. We conclude that the role of SST in the QBO–MJO connection might either be driven by ENSO or be independent of it.

The inability of our analysis to demonstrate conclusively that the SST, or ENSO specifically, controls (or does not control) both the phase of the QBO and the MJO power, is largely a result of the limited length of the observational record from the satellite period (1979–2014) for which the stratospheric data may be more reliable. This limited record is likely not long enough to average out short-term noise signals that may introduce spurious correlations or mask relations between the QBO, MJO, the SST, and perhaps ENSO.

To further examine the SST–QBO–MJO connection, we studied simulations with a coupled global model, 83LCESM2, which successfully simulates the MJO, ENSO, and QBO. The QBO–MJO connection is not captured by the coupled model, despite its ability to simulate some of the key processes involved. While the simulated La Niña and El Niño signals are reasonably strong, the simulated QBOE SST anomaly does not resemble the simulated La Niña SST anomaly, in strong contrast to what we find in the observations. We speculate that the lack of a realistic QBOE SST signal in the coupled model may explain the failure of the coupled model to simulate the QBO–MJO connection.

We then attempted to analyze the possible contribution of the SST to the QBO–MJO connection by examining the difference in MJO power between atmospheric-only simulations driven by observed composited QBOE and QBOW SSTs. The MJO power in these simulations appears to show a weak signal that is qualitatively similar to the observed MJO's response to

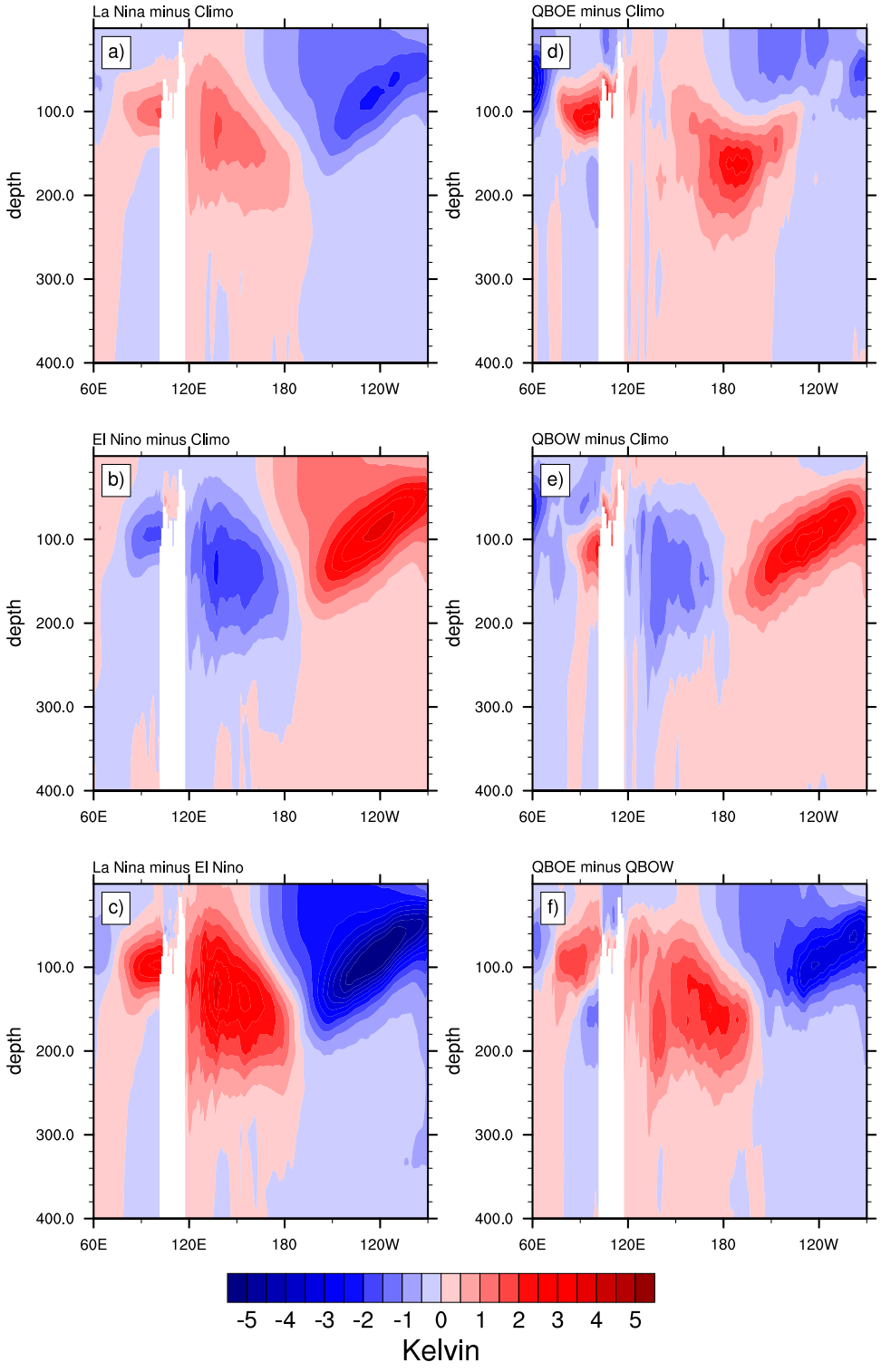

FIG. 12. Observed subsurface upper-ocean temperature along the equator (5°S–5°N) in the Indian and Pacific Oceans for (a) La Niña minus climatology, (b) El Niño minus climatology, (c) La Niña minus El Niño, (d) QBOE minus climatology, (e) QBOW minus climatology, and (f) QBOE minus QBOW.

the QBO. While these results are not conclusive, we pointed out that models do tend to produce unrealistically weak MJOs when run with prescribed SSTs and that this may at least partially explain the weak MJO response to the QBO SSTs. While our coupled model simulation joins the ranks of the previous attempts to use imperfect models to study the QBO–MJO connection (Kim et al. 2020; Martin et al. 2021a,c), our fixed-SST experiments show some interesting signals consistent with a role for the SST seen in observations.

Our results suggest many possibilities to investigate the physical mechanisms behind this link. We have suggested that a small QBO-related surface wind stress may lead to a shift of thermocline water in the upper ocean, which may also affect the SST. A surface-wind signal of the QBO may also lead to a change in the surface latent heat flux, also potentially affecting the tropical SST. The QBO's effect on upper-tropospheric winds may influence cloudiness by advecting MJO-related clouds, which can affect surface solar radiation and thus the SST.

Our work also raises many questions regarding the causality behind the correlations we identified. Why are the La Niña and QBOE SSTs so highly correlated? Does a QBOE state enhance the probability of La Niña conditions? Or does a La Niña state lead to a QBOE? Does the MJO play a role in this synchronization, or is the observed QBO–MJO connection just a side effect of a partially synchronized ENSO and QBO variability? Future work will address these questions.

Acknowledgments. We thank George Kiladis and two anonymous reviewers for their detailed and constructive comments, which led to major improvements in the paper. This work was funded by the U.S. National Science Foundation (NSF) Award AGS-1826643 to Colorado State University (author Randall and Branson), NSF Climate Dynamics program Grant AGS-1826635 (author Tziperman), and the Lorenz-Houghton Fellowship provided to author Kang by the Earth, Atmospheric, and Planetary Sciences Department of the Massachusetts Institute of Technology. Tziperman thanks the Weizmann Institute for its hospitality during parts of this work. We thank the CESM Vertical Grid Task Team led by Isla Simpson for developing the 83LCESM and carrying out the coupled simulation that we have analyzed. The CESM project is supported primarily by the NSF. Part of the computing and data storage resources, including the Cheyenne supercomputer (doi:10.5065/D6RX99HX), were provided by the Computational and Information Systems Laboratory (CISL) at the National Center for Atmospheric Research, which is a major facility sponsored by the National Science Foundation under Cooperative Agreement 1852977. Portions of this study were supported by the Regional and Global Model Analysis (RGMA) component of the Earth and Environmental System Modeling Program of the U.S. Department of Energy's Office of Biological and Environmental Research (BER) via National Science Foundation IA 1844590.

Data availability statement. All observations used in this study are openly available as follows. The ERA-Interim reanalysis is available from the European Centre for Medium-Range Weather Forecasts (Dee et al. 2011). NOAA OLR data are available as discussed in Schreck et al. (2018) and Wang et al. (2021). The ORAP5 ocean reanalysis is available from ECMWF and is described by Zuo et al. (2017). The model used is the Community Earth System Model, version 2 (CESM2), developed by the CESM Vertical Grid Task Team, and is available from the National Center for Atmospheric Research. The model output used in this paper is too large to be publicly archived with available resources and is freely available to download upon request from the corresponding author.

REFERENCES

Arnold, N. P., M. Branson, M. A. Burt, D. S. Abbot, Z. Kuang, D. A. Randall, and E. Tziperman, 2014: Effects of explicit atmospheric convection at high CO_2. *Proc. Natl. Acad. Sci. USA*, **111**, 10 943–10 948, https://doi.org/10.1073/pnas.1407175111.

——, ——, Z. Kuang, D. A. Randall, and E. Tziperman, 2015: MJO intensification with warming in the super-parameterized CESM. *J. Climate*, **28**, 2706–2724, https://doi.org/10.1175/JCLI-D-14-00494.1.

Baldwin, M. P., and T. J. Dunkerton, 2001: Stratospheric harbingers of anomalous weather regimes. *Science*, **294**, 581–584, https://doi.org/10.1126/science.1063315.

Bjerknes, J., 1969: Atmospheric teleconnections from the equatorial Pacific. *Mon. Wea. Rev.*, **97**, 163–172, https://doi.org/10.1175/1520-0493(1969)097<0163:ATFTEP>2.3.CO;2.

Bretherton, C. S., C. Smith, and J. M. Wallace, 1992: An intercomparison of methods for finding coupled patterns in climate data. *J. Climate*, **5**, 541–560, https://doi.org/10.1175/1520-0442(1992)005<0541:AIOMFF>2.0.CO;2.

Bui, H. X., and E. D. Maloney, 2018: Changes in Madden-Julian Oscillation precipitation and wind variance under global warming. *Geophys. Res. Lett.*, **45**, 7148–7155, https://doi.org/10.1029/2018GL078504.

Cassou, C., 2008: Intraseasonal interaction between the Madden-Julian Oscillation and the North Atlantic Oscillation. *Nature*, **455**, 523–527, https://doi.org/10.1038/nature07286.

Chen, X., C. Li, and Y. Tan, 2015: The influence of El Niño on MJO over the equatorial Pacific. *J. Ocean Univ. China*, **14** (1), 1–8, https://doi.org/10.1007/s11802-015-2381-y.

Christiansen, B., S. Yang, and M. S. Madsen, 2016: Do strong warm ENSO events control the phase of the stratospheric QBO? *Geophys. Res. Lett.*, **43**, 10 489–10 495, https://doi.org/10.1002/2016GL070751.

Danabasoglu, G., and Coauthors, 2020: The Community Earth System Model version 2 (CESM2). *J. Adv. Model. Earth Syst.*, **12**, e2019MS001916, https://doi.org/10.1029/2019MS001916.

Dee, D. P., and Coauthors, 2011: The ERA-Interim reanalysis: Configuration and performance of the data assimilation system. *Quart. J. Roy. Meteor. Soc.*, **137**, 553–597, https://doi.org/10.1002/qj.828.

Dunkerton, T. J., and D. P. Delisi, 1985: Climatology of the equatorial lower stratosphere. *J. Atmos. Sci.*, **42**, 376–396, https://doi.org/10.1175/1520-0469(1985)042<0376:COTELS>2.0.CO;2.

Eisenman, I., L. Yu, and E. Tziperman, 2005: Westerly wind bursts: ENSO's tail rather than the dog? *J. Climate*, **18**, 5224–5238, https://doi.org/10.1175/JCLI3588.1.

Garfinkel, C. I., and D. L. Hartmann, 2007: Effects of the El Niño–Southern Oscillation and the quasi-biennial oscillation on polar temperatures in the stratosphere. *J. Geophys. Res.*, **112**, D19112, https://doi.org/10.1029/2007JD008481.

Geller, M. A., T. Zhou, and W. Yuan, 2016: The QBO, gravity waves forced by tropical convection, and ENSO. *J. Geophys. Res. Atmos.*, **121**, 8886–8895, https://doi.org/10.1002/2015JD024125.

Gettelman, A., and Coauthors, 2019: The Whole Atmosphere Community Climate Model version 6 (WACCM6). *J. Geophys. Res. Atmos.*, **124**, 12 380–12 403, https://doi.org/10.1029/2019JD030943.

Goss, M., S. B. Feldstein, and S. Lee, 2016: Stationary wave interference and its relation to tropical convection and Arctic warming. *J. Climate*, **29**, 1369–1389, https://doi.org/10.1175/JCLI-D-15-0267.1.

Gray, L. J., J. A. Anstey, Y. Kawatani, H. Lu, S. Osprey, and V. Schenzinger, 2018: Surface impacts of the Quasi Biennial Oscillation. *Atmos. Chem. Phys.*, **18**, 8227–8247, https://doi.org/10.5194/acp-18-8227-2018.

Harrison, D. E., and P. S. Schopf, 1984: Kelvin-wave-induced anomalous advection and the onset of surface warming in El Niño event. *Mon. Wea. Rev.*, **112**, 923–933, https://doi.org/10.1175/1520-0493(1984)112<0923:KWIAAA>2.0.CO;2.

Hendon, H. H., C. Zhang, and J. D. Glick, 1999: Interannual variation of the Madden–Julian oscillation during austral summer. *J. Climate*, **12**, 2538–2550, https://doi.org/10.1175/1520-0442(1999)012<2538:IVOTMJ>2.0.CO;2.

Hu, Z.-Z., B. Huang, J. L. Kinter III, Z. Wu, and A. Kumar, 2012: Connection of the stratospheric QBO with global atmospheric general circulation and tropical SST. Part II: Interdecadal variations. *Climate Dyn.*, **38**, 25–43, https://doi.org/10.1007/s00382-011-1073-6.

Huang, K., J. H. Richter, and K. V. Pegion, 2023: Captured QBO-MJO connection in a subseasonal prediction system. *Geophys. Res. Lett.*, **50**, e2022GL102648, https://doi.org/10.1029/2022GL102648.

Jones, C., and L. M. V. Carvalho, 2006: Changes in the activity of the Madden–Julian oscillation during 1958–2004. *J. Climate*, **19**, 6353–6370, https://doi.org/10.1175/JCLI3972.1.

Kang, W., and E. Tziperman, 2017: More frequent sudden stratospheric warming events due to enhanced MJO forcing expected in a warmer climate. *J. Climate*, **30**, 8727–8743, https://doi.org/10.1175/JCLI-D-17-0044.1.

——, and ——, 2018: The role of zonal asymmetry in the enhancement and suppression of sudden stratospheric warming variability by the Madden-Julian Oscillation. *J. Climate*, **31**, 2399–2415, https://doi.org/10.1175/JCLI-D-17-0489.1.

Kiladis, G. N., K. H. Straub, G. C. Reid, and K. S. Gage, 2001: Aspects of interannual and intraseasonal variability of the tropopause and lower stratosphere. *Quart. J. Roy. Meteor. Soc.*, **127**, 1961–1983, https://doi.org/10.1002/qj.49712757606.

Kim, H., J. M. Caron, J. H. Richter, and I. R. Simpson, 2020: The lack of QBO-MJO connection in CMIP6 models. *Geophys. Res. Lett.*, **47**, e2020GL087295, https://doi.org/10.1029/2020GL087295.

Lee, J. C. K., and N. P. Klingaman, 2018: The effect of the Quasi-Biennial Oscillation on the Madden–Julian oscillation in the met office unified model global ocean mixed layer configuration. *Atmos. Sci. Lett.*, **19**, e816, https://doi.org/10.1002/asl.816.

Lim, Y., and S.-W. Son, 2020: QBO-MJO connection in CMIP5 models. *J. Geophys. Res. Atmos.*, **125**, e2019JD032157, https://doi.org/10.1029/2019JD032157.

Lin, J., and K. Emanuel, 2023: Stratospheric modulation of the MJO through cirrus cloud feedbacks. *J. Atmos. Sci.*, **80**, 273–299, https://doi.org/10.1175/JAS-D-22-0083.1.

Liu, P., T. Li, B. Wang, M. Zhang, J.-J. Luo, Y. Masumoto, X. Wang, and E. Roeckner, 2013: MJO change with A1B global warming estimated by the 40-km ECHAM5. *Climate Dyn.*, **41**, 1009–1023, https://doi.org/10.1007/s00382-012-1532-8.

Madden, R. A., and P. R. Julian, 1971: Detection of a 40-50 day oscillation in zonal wind in tropical Pacific. *J. Atmos. Sci.*, **28**, 702–708, https://doi.org/10.1175/1520-0469(1971)028<0702:DOADOI>2.0.CO;2.

Marshall, A. G., H. H. Hendon, S.-W. Son, and Y. Lim, 2017: Impact of the quasi-biennial oscillation on predictability of the Madden–Julian Oscillation. *Climate Dyn.*, **49**, 1365–1377, https://doi.org/10.1007/s00382-016-3392-0.

Martin, Z., S. Wang, J. Nie, and A. Sobel, 2019: The impact of the QBO on MJO convection in cloud-resolving simulations. *J. Atmos. Sci.*, **76**, 669–688, https://doi.org/10.1175/JAS-D-18-0179.1.

——, F. Vitart, S. Wang, and A. Sobel, 2020: The impact of the stratosphere on the MJO in a forecast model. *J. Geophys. Res. Atmos.*, **125**, e2019JD032106, https://doi.org/10.1029/2019JD032106.

——, C. Orbe, S. Wang, and A. Sobel, 2021a: The MJO–QBO relationship in a GCM with stratospheric nudging. *J. Climate*, **34**, 4603–4624, https://doi.org/10.1175/JCLI-D-20-0636.1.

——, A. Sobel, A. Butler, and S. Wang, 2021b: Variability in QBO temperature anomalies on annual and decadal time scales. *J. Climate*, **34**, 589–605, https://doi.org/10.1175/JCLI-D-20-0287.1.

——, S.-W. Son, A. Butler, H. Hendon, H. Kim, A. Sobel, S. Yoden, and C. Zhang, 2021c: The influence of the quasi-biennial oscillation on the Madden–Julian oscillation. *Nat. Rev. Earth Environ.*, **2**, 477–489, https://doi.org/10.1038/s43017-021-00173-9.

McPhaden, M. J., 1999: Genesis and evolution of the 1997-98 El Niño. *Science*, **283**, 950–954, https://doi.org/10.1126/science.283.5404.950.

Meehl, G. A., and Coauthors, 2021: Initialized Earth system prediction from subseasonal to decadal timescales. *Nat. Rev. Earth Environ.*, **2**, 340–357, https://doi.org/10.1038/s43017-021-00155-x.

Miyakawa, T., H. Yashiro, T. Suzuki, H. Tatebe, and M. Satoh, 2017: A Madden-Julian Oscillation event remotely accelerates ocean upwelling to abruptly terminate the 1997/1998 super El Niño. *Geophys. Res. Lett.*, **44**, 9489–9495, https://doi.org/10.1002/2017GL074683.

Nishimoto, E., and S. Yoden, 2017: Influence of the stratospheric quasi-biennial oscillation on the Madden–Julian oscillation during austral summer. *J. Atmos. Sci.*, **74**, 1105–1125, https://doi.org/10.1175/JAS-D-16-0205.1.

Oliver, E. C. J., and K. R. Thompson, 2012: A reconstruction of Madden–Julian oscillation variability from 1905 to 2008. *J. Climate*, **25**, 1996–2019, https://doi.org/10.1175/JCLI-D-11-00154.1.

Pang, B., Z. Chen, Z. Wen, and R. Lu, 2016: Impacts of two types of El Niño on the MJO during boreal winter. *Adv. Atmos. Sci.*, **33**, 979–986, https://doi.org/10.1007/s00376-016-5272-2.

Rushley, S. S., D. Kim, and Á. F. Adames, 2019: Changes in the MJO under greenhouse gas–induced warming in CMIP5 models. *J. Climate*, **32**, 803–821, https://doi.org/10.1175/JCLI-D-18-0437.1.

Saji, N. H., B. N. Goswami, P. N. Vinayachandran, and T. Yamagata, 1999: A dipole mode in the tropical Indian Ocean. *Nature*, **401**, 360–363, https://doi.org/10.1038/43854.

Sakaeda, N., J. Dias, and G. N. Kiladis, 2020: The unique characteristics and potential mechanisms of the MJO-QBO relationship. *J. Geophys. Res. Atmos.*, **125**, e2020JD033196, https://doi.org/10.1029/2020JD033196.

Schirber, S., 2015: Influence of ENSO on the QBO: Results from an ensemble of idealized simulations. *J. Geophys. Res. Atmos.*, **120**, 1109–1122, https://doi.org/10.1002/2014JD022460.

Schreck, C. J., III, H.-T. Lee, and K. R. Knapp, 2018: HIRS outgoing longwave radiation—Daily climate data record: Application toward identifying tropical subseasonal variability. *Remote Sens.*, **10**, 1325, https://doi.org/10.3390/rs10091325.

Schubert, J. J., B. Stevens, and T. Crueger, 2013: Madden-Julian Oscillation as simulated by the MPI Earth system model: Over the last and into the next millennium. *J. Adv. Model. Earth Syst.*, **5**, 71–84, https://doi.org/10.1029/2012MS000180.

Seiki, A., and Y. N. Takayabu, 2007: Westerly wind bursts and their relationship with intraseasonal variations and ENSO. Part I: Statistics. *Mon. Wea. Rev.*, **135**, 3325–3345, https://doi.org/10.1175/MWR3477.1.

Slingo, J. M., D. P. Rowell, K. R. Sperber, and F. Nortley, 1999: On the predictability of the interannual behaviour of the Madden-Julian Oscillation and its relationship with El Niño. *Quart. J. Roy. Meteor. Soc.*, **125**, 583–609, https://doi.org/10.1256/smsqj.55410.

Son, S.-W., Y. Lim, C. Yoo, H. H. Hendon, and J. Kim, 2017: Stratospheric control of the Madden–Julian oscillation. *J. Climate*, **30**, 1909–1922, https://doi.org/10.1175/JCLI-D-16-0620.1.

Subramanian, A., M. Jochum, A. J. Miller, R. Neale, H. Seo, D. Waliser, and R. Murtugudde, 2014: The MJO and global warming: A study in CCSM4. *Climate Dyn.*, **42**, 2019–2031, https://doi.org/10.1007/s00382-013-1846-1.

Sun, L., H. Wang, and F. Liu, 2019: Combined effect of the QBO and ENSO on the MJO. *Atmos. Ocean. Sci. Lett.*, **12**, 170–176, https://doi.org/10.1080/16742834.2019.1588064.

Sweeney, A., Q. Fu, H. A. Pahlavan, and P. Haynes, 2023: Seasonality of the QBO impact on equatorial clouds. *J. Geophys. Res. Atmos.*, **128**, e2022JD037737, https://doi.org/10.1029/2022JD037737.

Taguchi, M., 2010: Observed connection of the stratospheric quasi-biennial oscillation with El Niño–Southern Oscillation in radiosonde data. *J. Geophys. Res.*, **115**, D18120, https://doi.org/10.1029/2010JD014325.

Tang, Y., and B. Yu, 2008: MJO and its relationship to ENSO. *J. Geophys. Res.*, **113**, D14106, https://doi.org/10.1029/2007JD009230.

Wang, L., T. Li, L. Chen, S. K. Behera, and T. Nasuno, 2018: Modulation of the MJO intensity over the equatorial western Pacific by two types of El Niño. *Climate Dyn.*, **51**, 687–700, https://doi.org/10.1007/s00382-017-3949-6.

Wang, T., and Coauthors, 2021: Validation of near-real-time NOAA-20 CrIS outgoing longwave radiation with multi-satellite datasets on broad timescales. *Remote Sens.*, **13**, 3912, https://doi.org/10.3390/rs13193912.

Wheeler, M., and G. N. Kiladis, 1999: Convectively coupled equatorial waves: Analysis of clouds and temperature in the wavenumber-frequency domain. *J. Atmos. Sci.*, **56**, 374–399, https://doi.org/10.1175/1520-0469(1999)056<0374:CCEWAO>2.0.CO;2.

Woolnough, S. J., F. Vitart, and M. A. Balmaseda, 2007: The role of the ocean in the Madden–Julian Oscillation: Implications for MJO prediction. *Quart. J. Roy. Meteor. Soc.*, **133**, 117–128, https://doi.org/10.1002/qj.4.

Yoo, C., and S.-W. Son, 2016: Modulation of the boreal wintertime Madden-Julian Oscillation by the stratospheric Quasi-Biennial Oscillation. *Geophys. Res. Lett.*, **43**, 1392–1398, https://doi.org/10.1002/2016GL067762.

——, S. Feldstein, and S. Lee, 2011: The impact of the Madden-Julian Oscillation trend on the Arctic amplification of surface air temperature during the 1979–2008 boreal winter. *Geophys. Res. Lett.*, **38**, L24804, https://doi.org/10.1029/2011GL049881.

——, S. Lee, and S. B. Feldstein, 2012a: Arctic response to an MJO-like tropical heating in an idealized GCM. *J. Atmos. Sci.*, **69**, 2379–2393, https://doi.org/10.1175/JAS-D-11-0261.1.

——, ——, and ——, 2012b: Mechanisms of Arctic surface air temperature change in response to the Madden–Julian oscillation. *J. Climate*, **25**, 5777–5790, https://doi.org/10.1175/JCLI-D-11-00566.1.

Yu, L., R. A. Weller, and W. T. Liu, 2003: Case analysis of a role of ENSO in regulating the generation of westerly wind bursts in the western equatorial Pacific. *J. Geophys. Res.*, **108**, 3128, https://doi.org/10.1029/2002JC001498.

Yuan, W., M. A. Geller, and P. T. Love, 2014: ENSO influence on QBO modulations of the tropical tropopause. *Quart. J. Roy. Meteor. Soc.*, **140**, 1670–1676, https://doi.org/10.1002/qj.2247.

Zhang, C., 2005: Madden-Julian Oscillation. *Rev. Geophys.*, **43**, RG2003, https://doi.org/10.1029/2004RG000158.

——, and B. Zhang, 2018: QBO-MJO connection. *J. Geophys. Res. Atmos.*, **123**, 2957–2967, https://doi.org/10.1002/2017JD028171.

Zhao, Y., and S. Nigam, 2015: The Indian Ocean dipole: A monopole in SST. *J. Climate*, **28**, 3–19, https://doi.org/10.1175/JCLI-D-14-00047.1.

Zuo, H., M. A. Balmaseda, and K. Mogensen, 2017: The new eddy-permitting ORAP5 ocean reanalysis: Description, evaluation and uncertainties in climate signals. *Climate Dyn.*, **49**, 791–811, https://doi.org/10.1007/s00382-015-2675-1.